RSC Advances

PAPER

View Article Online
View Journal | View Issue

Cite this: *RSC Adv.*, 2023, **13**, 26149

Anomalous catalytic and antibacterial activity confirmed by molecular docking analysis of silver and polyacrylic acid doped CeO_2 nanostructures†

Muhammad Ikram, *[a] Rizwan Karim,[b] Ali Haider, [c] Anum Shahzadi,[d] Mohammed M. Algaradah,[e] Anwar Ul-Hamid, *[f] Walid Nabgan, [g] Ahmed M. Fouda[h] and Salamat Ali[b]

Received 15th July 2023
Accepted 26th August 2023

DOI: 10.1039/d3ra04760a

rsc.li/rsc-advances

This research presents the novel synthesis of CeO_2 nanostructures (NSs) doped with a fixed amount of capping agent (polyacrylic acid-PAA) and different concentrations (0.01 and 0.03) of silver (Ag). This work aimed to examine the catalytic and antibacterial efficacy with evidential molecular docking analysis of Ag/PAA doped CeO_2. Systematic characterization was used to analyze the effect of Ag and a capping agent on crystal structure, morphology, absorbance wavelength, and the exciton recombination rate of CeO_2. The silver metal and capping agent (PAA) were added into CeO_2 to reduce the size of NSs, enhancing the catalytic efficacy. These binary dopants (Ag–PAA) based CeO_2 revealed remarkable results for catalytic de-colorization of rhodamine B dye and antimicrobial potential as the dopants provide more active sites. Notably, (0.03) Ag/PAA doped CeO_2 NSs exhibited a substantial catalytic reduction (98.9%) of rhodamine B dye in an acidic medium. The higher doped CeO_2 revealed a significant inhibition zone (3.75 mm) against *Escherichia coli* at maximal concentration. Furthermore, *in silico* docking showed the possible inhibitory impact of produced nanomaterials on the fatty acid biosynthesis enzymes FabI and FabH.

1. Introduction

Water is crucial for the existence of life on our planet. The pollution caused by wastewater from human activities negatively impacts people and the ecosystem. Many industries, such as textiles, printing, dyeing plastic, and health laboratories, are releasing various kinds of dyes into the freshwater streams, affecting the environment.[1,2] The dye production can range from 1 00 000 to 7 00 000 metric tons annually. Almost 70 000 tons of effluents are directly discarded into the environment by underdeveloped countries. Different cationic and anionic dyes in sewage include rhodamine B (RhB), methylene orange, triphenylmethane, methylene blue, and phenothiazine.[3] RhB is a cationic dye that causes several human health problems and threatens aquatic life.[4] Various physical, chemical, and biological methods have been used to degrade RhB dye from water. Such methods include adsorption,[5] reverse osmosis,[6] coagulation,[7,8] biological,[9] and photochemical degradation[10] for the treatment of dyes in water. However, these technologies have several drawbacks, including cost and complex procedures. Recently, catalytic activity (CA) of metal oxides has stimulated researchers and produced interest due to its low toxicity and cost-effective behavior.

Many bacteria, such as *Escherichia coli* (*E. coli*) and *Pseudomonas aeruginosa*, cause health problems.[11] *E. coli* includes commercial strains and causes many human diseases, resulting in more than 2 million deaths yearly.[12] In recent decades, inorganic semiconductor nanomaterials have been found with physicochemical properties, environmental sustainability, and non-toxicity.[13] Rare earth metal oxides (REMOs) and transition metal oxides (TMOs), mainly ZnO, CdO, La_2O_3, CeO_2, TiO_2, Cu_2O zerovalent metals, and iron oxide, act as efficient co-catalysts in the degradation of certain dyes.[14,15] These metal oxides have a useful role in optics and medicine,[16] Whereas CeO_2 has attracted the attention of many researchers due to less toxicity, broadband gap energy (E_g), excellent stability, and considerable CA.[17]

[a]*Solar Cell Applications Research Lab, Department of Physics, Government College University Lahore, Lahore, 54000, Punjab, Pakistan. E-mail: dr.muhammadikram@gcu.edu.pk*

[b]*Department of Physics, Riphah Institute of Computing and Applied Sciences (RICAS), Riphah International University, 14 Ali Road, Lahore, Pakistan*

[c]*Department of Clinical Sciences, Faculty of Veterinary and Animal Sciences, Muhammad Nawaz Shareef University of Agriculture, Multan, 66000, Pakistan*

[d]*Faculty of Pharmacy, The University of Lahore, 54000, Pakistan*

[e]*Chemistry Department, King Khalid Military Academy, Riyadh 11495, Saudi Arabia*

[f]*Core Research Facilities, Research Institute, King Fahd University of Petroleum & Minerals, Dhahran, 31261, Saudi Arabia. E-mail: anwar@kfupm.edu.sa*

[g]*Departament d'Enginyeria Química, Universitat Rovira i Virgili, Av Països Catalans 26, 43007, Tarragona, Spain. E-mail: walid.nabgan@urv.cat*

[h]*Chemistry Department, Faculty of Science, King Khalid University, Abha 61413, Saudi Arabia*

† Electronic supplementary information (ESI) available. See DOI: https://doi.org/10.1039/d3ra04760a

The thermodynamic and thermo-physical mechanical properties and elastic behavior increased the importance of CeO_2 in fuel development.[18] CeO_2 can be used as oxygen ion conductors in solid oxide fuel cells, ultraviolet blocking sheets (UV shielding), three-way catalysts for treating automobile exhaust gas, and polishing agents for chemical mechanical planarization.[19–23] Intrinsic oxygen vacancies are generated with CeO_2, which increases the charge transfer to enhance the electrochemical performance.[24,25]

The degradation efficacy can be enhanced by adding polymers like PAA, chitosan, and starch into CeO_2. PAA was used as a dopant possessing significant degradation properties and reducing the recombination rate of CeO_2.[26,27] Several methods and elements are reported for organic treatment, including Ag nanoparticle's vigorous antimicrobial properties, which can kill numerous bacteria.[11] Ag and CeO_2 can exhibit a relatively large surface area of nanocomposites, enhancing the CA.[28] The current research aims to investigate the antimicrobial and degrading ability of various concentrations of Ag-doped into a fixed amount of binary system composed of PAA-doped CeO_2 NSs.

2. Experimental part

2.1 Materials

$Ce(NO_3)_3 \cdot 6H_2O$, poly(acrylic acid $(C_3H_4O_2))_n$, $AgNO_3$, and NaOH were procured from Sigma-Aldrich.

2.2 Synthesis of Ag and PAA doped CeO_2

0.5 M of $Ce(NO_3)_3 \cdot 6H_2O$ was used to prepare CeO_2 NSs by co-precipitation approach under robust stirring at 65 °C for 40 min. The precipitating agent (NaOH) was added dropwise in stirred solution to form metal hydroxides by maintaining the pH ~ 12. Moreover, obtained precipitates were centrifuged twice at 7500 rpm for 8 min, dried at 140 °C for 12 h, and crushed to obtain a powder. For doping, (0.01 and 0.03) of Ag and a fixed amount (0.02) of PAA–CeO_2 NSs were prepared using the same method (Fig. 1). The prepared samples CeO_2, PAA–CeO_2, Ag (0.01) doped PAA–CeO_2 and Ag (0.03) doped PAA–CeO_2 are represented in the further part of the manuscript such as (0–1), 0.02–1, 0.01:0.02–1, 0.03:0.02–1 respectively.

2.3 Catalytic activity (CA)

The CA of dopant-free and Ag/PAA added into CeO_2 were analyzed in the occurrence of $NaBH_4$ to degrade the RhB. Firstly, the 400 μL of $NaBH_4$ was integrated with 3 mL of RhB solution, followed by incorporating the 400 μL of CeO_2 and (0.01 and 0.03) of Ag/PAA doped CeO_2. The dye de-colorization was conducted by reduction of RhB. The reducing agent ($NaBH_4$) caused the reduction of RhB into leuco rhodamine B (LRhB). The de-colorization of RhB was observed at different times using of UV-Vis spectrophotometer.

2.4 Separation and identification of MDR *E. coli*

2.4.1 Sample collection. Sample milk was collected from the diary centers in distilled containers and transported to the laboratory at low temperatures. Enumeration of coliforms in the sample milk was performed on MacConkey agar then plates were nurtured at 37 °C for a day.

2.4.2 Identification of bacterial isolates. Initially, MDR *E. coli* were identified by physical and chemical tests regarding Bergey's Manual of Determinative Bacteriology.

2.5 Antimicrobial activity

The agar well diffusion method was used to assess the antimicrobial activity of CeO_2, and (0.01 & 0.03) Ag/PAA doped CeO_2 through inhibition zones against MDR *E. coli*. MDR *E. coli* bacteria at a 1.5×10^8 CFU mL^{-1} concentration were inoculated onto MacConkey agar plates. Sterile cork borers were used to create 6 mm diameter holes in the agar plates. A range of pristine and doped CeO_2 NSs concentrations was used to fill the wells, including (0.5 mg/50 μL) and (1.0 mg/50 μL). Deionized (DI) water (50 μL) was utilized as the negative control, and the positive control was ciprofloxacin (0.005 mg/50 μL).

2.5.1 Minimum inhibitory concentration (MIC) test. The minimum inhibitory concentration (MIC) of CeO_2 and Ag/PAA doped NSs was determined using broth's conventional twofold serial dilution method. MDR *E. coli* isolates were grown in broth at 37 °C for 18 h. We used the McFarland standard of 0.5 for the turbidity of MDR *E. coli* specimens. The inoculums were made by diluting the original solution by a factor of 10 with broth containing 10^7 CFU mL^{-1}. The initial dispersion quantity of 100 mg L^{-1} of CeO_2 and Ag/PAA doped NSs was diluted serially by a factor of 2. Later, the bacterium suspensions were injected into sterile tubes containing the serial twofold dilution solution, and the whole process was done under strict sterile conditions. The minimum inhibitory concentration (MIC) in each example was defined as the lowest antibacterial concentration that prevented detectable growth after incubation at 37 °C for 18 h.

2.6 Molecular docking analysis

Molecular docking was performed on the enzymes enoyl-[acyl-carrier-protein] reductase (FabI) and -ketoacyl acyl carrier protein synthase III (FabH) from *Escherichia coli*, both of which play important roles in fatty acids pathways. The 3D structures of FabH (PDB ID 5BNM)[29] and FabI (PDB ID 1MFP)[30] were retrieved from Protein Data Bank. The molecular docking predictions were made using Sybyl X-2.0, as reported in previous studies.[31,32] Briefly, water molecules with native ligands were removed from the protein, and polar H-atoms were added to each molecule. The ligands were designed *via* a sketch module; then, energy was minimized. The binding pocket was determined within 5 Å of the endogenous ligand. The ten best-docked complexes were selected from each set of possible outcomes. Pymol was used to create a three-dimensional depiction of binding interactions.

2.7 Characterizations

The crystal structure and phase purity of CeO_2 and Ag/PAA doped CeO_2 were assessed through a PANalytical Xpert PRO XRD system utilizing CuKα radiation (λ ~0.154 nm) in 2θ range

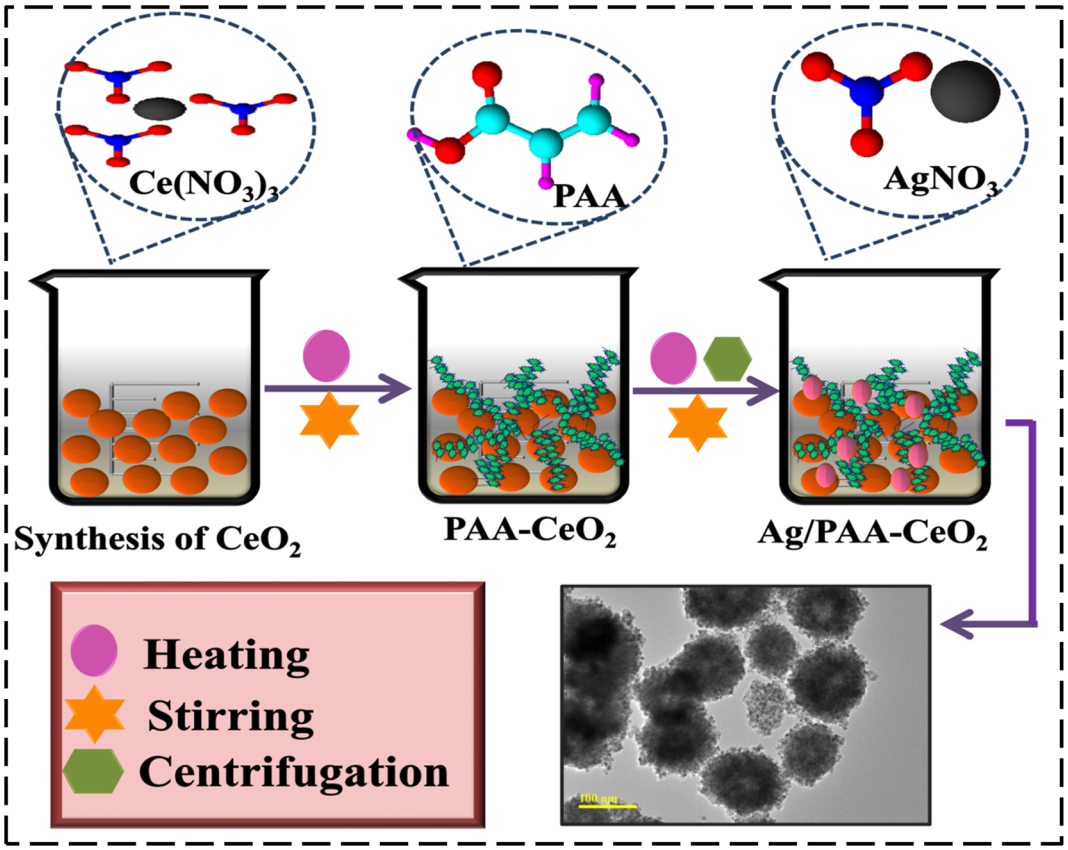

Fig. 1 Synthesis of Ag/PAA doped CeO_2 NSs.

20–70°. The optical features of prepared NSs were investigated through UV-Vis LABDeX spectrophotometer with range from 260 to 500 nm. FTIR PerkinElmer 3100 spectrometer was used in the wavenumber range from 4000 to 500 cm^{-1} to determine the vibrational modes of the prepared catalyst. The morphological properties of CeO_2 and Ag/PAA doped NSs were examined through JSM-6460LV FE-SEM joined with EDS spectrometer.

3. Results and discussion

The crystal structure and phase identification of pure and Ag/PAA doped CeO_2 were investigated through XRD in the 2θ range from 20–65° as depicted in Fig. 2(a). Diffraction peaks at 28.55° (111), 33.08° (200), 47.47° (220), and 56.33° (311) revealed the cubic configuration of CeO_2 along space group $Fm\bar{3}m$ confirmed by (JCPDS card no. 00-034-0394). Upon incorporation of PAA, the crystallinity of NSs was reduced, attributed to the amorphous behavior of the polymer.[33] The intensity was further lowered by Ag doping may be associated with defects or disturbances in the cubic structure of CeO_2 affected by silver ion.[34] The crystallite size of CeO_2 and Ag/PAA doped CeO_2 were determined by Debye–Scherer equation:

$$D = \frac{0.9\lambda}{\beta \cos \theta} \quad (1)$$

where λ and β represent the X-ray wavelength and full-width half maxima of peaks and D is crystallite size. Upon doping of Ag and PAA, β (full width half maxima) increased and caused the reduction in crystallite size of prepared samples. The average crystallite size was decreased from 8.93 to 6.19 nm by adding Ag and PAA into CeO_2.

FTIR spectra were utilized to investigate the vibrational mode of CeO_2 and Ag/PAA doped NSs (Fig. 2(b)). Transmittance bands at 1630 and 3447 cm^{-1} were associated with bending and stretching modes of H_2O accordingly.[35,36] The bands at 1080 and 852 cm^{-1} manifested the vibrational stretch of Ce–O–C.[37,38] The band at 1384 cm^{-1} reflects undesired elements in the sample, specifically N–O stretching due to nitrates.[39] After adding Ag and PAA, no clear shift was detected in transmittance spectra. Furthermore, the SAED pattern of pristine and Ag/PAA incorporated CeO_2 exhibited bright rings associated with different XRD facets (111), (220), (311), and (200), as represented in Fig. 2(c–f).

The optical features of bare and Ag/PAA doped CeO_2 NSs were investigated through electronic spectra ranging from 260 to 550 nm, as depicted in Fig. 3(a). The absorption band of CeO_2 was observed between 280 and 330 nm, indicating the transfer of electrons from the 2p valence band of oxygen to the 4f conduction band of Ce^{4+}.[40,41] Upon addition of Ag and PAA, the bathochromic shift was observed assigned to reduction in E_g. By Tauc's equation, E_g was calculated to be 3.60, 3.53, 3.47, and

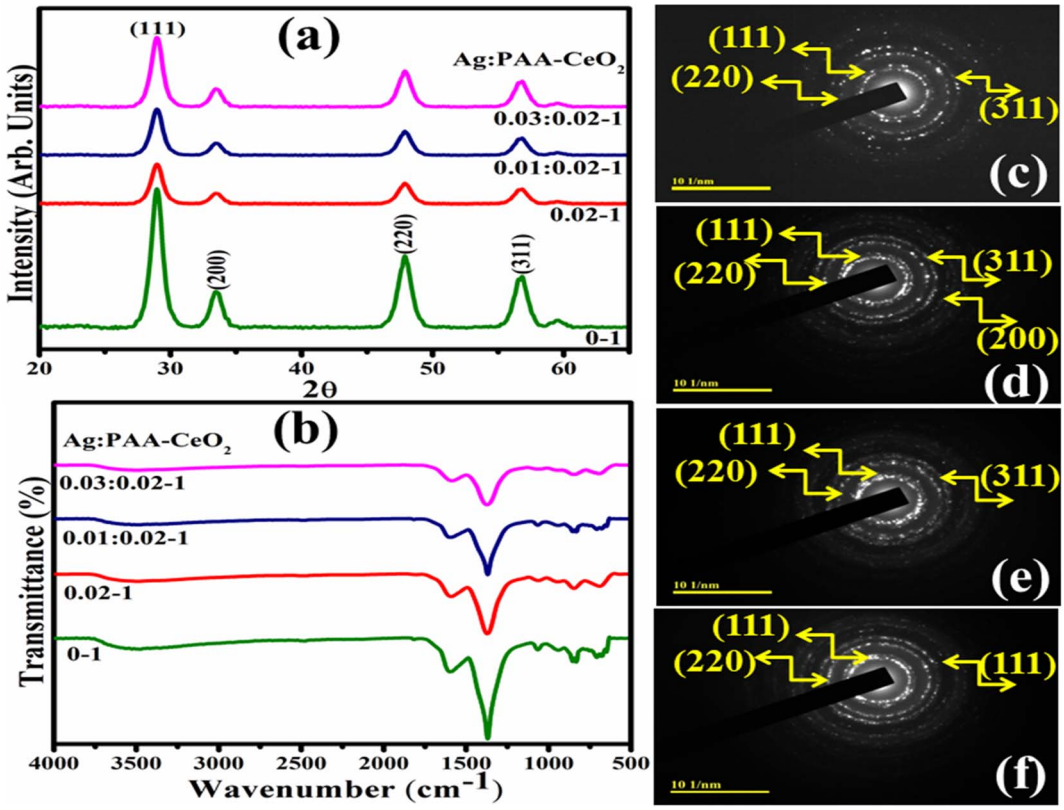

Fig. 2 (a) Diffraction pattern, (b) FTIR spectra of undoped and doped CeO_2, and (c–f) SAED analysis of CeO_2, PAA–CeO_2, (0.01) Ag/PAA–CeO_2 and (0.03) Ag/PAA doped CeO_2.

3.38 eV for CeO_2, PAA–CeO_2, (0.01) Ag/PAA–CeO_2 and (0.03) Ag/PAA–CeO_2, respectively (Fig. 3(b)).[42,43] PL spectroscopy investigated the quantum confinement effect and exciton recombination (Fig. 3(c)). CeO_2 NSs exhibited a strong emission band at 414 nm.[44] The PL intensity was diminished upon PAA, indicating a less exciton recombination rate and higher catalytic activity. The peak intensity was further reduced by Ag doping assigned to phosphorescence phenomena.[45]

TEM images investigate the morphology of CeO_2 and Ag/PAA doped CeO_2, as shown in Fig. 4(a–d). Fig. 4(a) exhibited the formation of agglomerated nanoparticles of CeO_2. The addition of a capping agent (PAA) led to forming a network of small-sized nanoparticles (NPs) that facilitated the movement of charge carriers during the catalytic process (Fig. 4(b)). The agglomerated NPs provided a significantly larger surface area, resulting in enhanced catalytic activity of CeO_2.[46] The addition of Ag resulted in the accumulation of NPs that exhibited an adhesive effect, causing them to adhere to one another along with PAA within CeO_2, as shown in Fig. 4(c and d).

HR-TEM microscopy was used to find the *d*-spacing of CeO_2 and Ag/PAA doped NSs, as exhibited in Fig. 5(a–d). The measured interlayer spacing value of pure and (0.01, 0.03) Ag/PAA incorporated CeO_2 was 0.31, 0.32, 0.33, and 0.34 nm, synchronized with XRD results.

The atomic distribution of host and Ag/PAA doped CeO_2 was determined by mapping results that revealed evenly distributed Ce, O, and Ag in the prepared sample (Fig. S1(a–d)†). EDS was utilized to evaluate the chemical configuration of the prepared catalyst (Fig. S1(a′–d′)†). The Ce and O peaks were detected, which verified the synthesis of CeO_2. Na peak in spectra was attributed to NaOH used to sustain the pH during the preparation of NSs.

The main components involved in the catalytic activity were reducing agent ($NaBH_4$), oxidizing agent (RhB dye) and catalysts (Ag/PAA doped CeO_2). The catalytic de-colorization of RhB in the existence of $NaBH_4$ was slow. Firstly, reducing agent ($NaBH_4$) splits into ions in which BH_4^- serves as a donor and H^+ as an electron acceptor. $NaBH_4$ accelerates the procedure and shortens the time required for triggering the pure and doped CeO_2 NSs by emitting H_2 from the reaction mixture (eqn (2)).

$$NaBH_4 + 2H_2O \rightarrow NaBO_2 + 8H_2 \quad (2)$$

The addition of pure and doped CeO_2 into RhB diminished the activation energy, thus increasing the reaction rate. The pure and Ag/PAA doped CeO_2 NSs are an electron relay system that facilitates electron transportation from the receiver ($NaBH_4$) to RhB. The electron is absorbed on the surface of RhB and de-colorized into LRhB (Fig. S2†).

The catalytic activity of CeO_2 and Ag/PAA doped CeO_2 NSs was determined through a UV-Vis spectrophotometer. The efficacy for de-colorization of RhB dye in acidic medium was 83.2, 87.8, 92.3 and 98.9%; in neutral medium 67.3, 70.2, 75.6

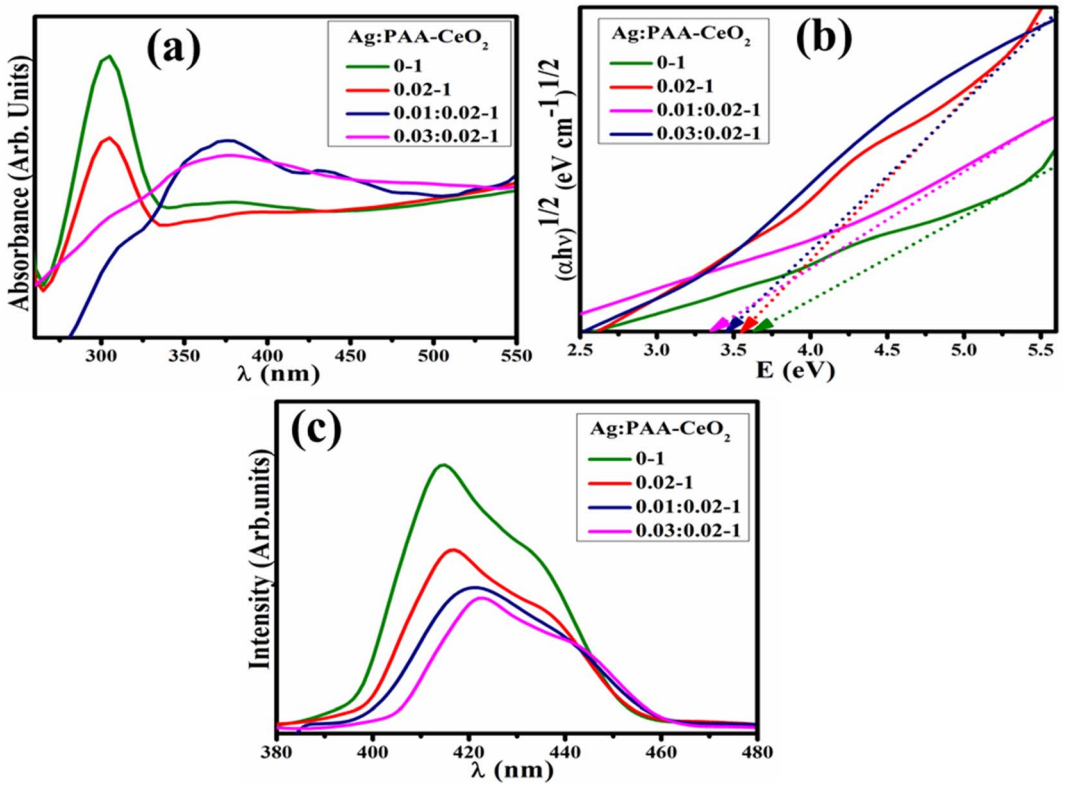

Fig. 3 (a) Electronic spectra, (b) Tauc plot and (c) PL spectra of pristine and (0.01, 0.03) Ag/PAA doped CeO_2.

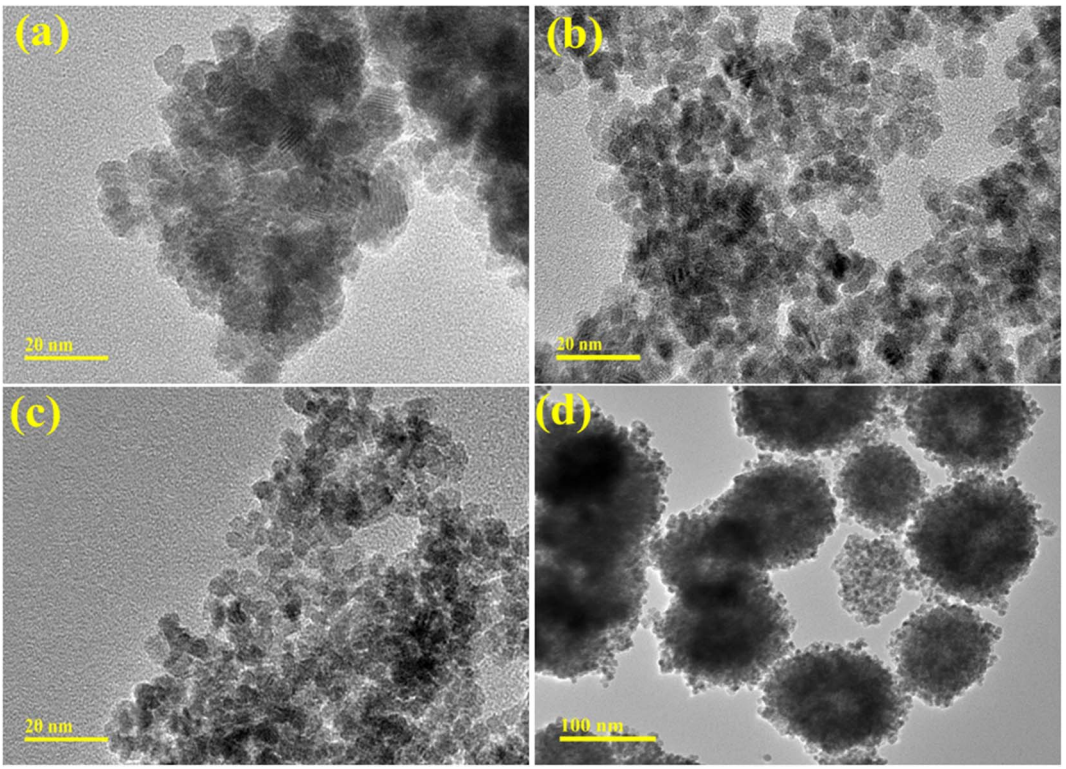

Fig. 4 TEM analysis of (a) CeO_2 (b) PAA-doped CeO_2 (c) 0.01 Ag/PAA doped CeO_2 (d) 0.03 Ag/PAA doped CeO_2.

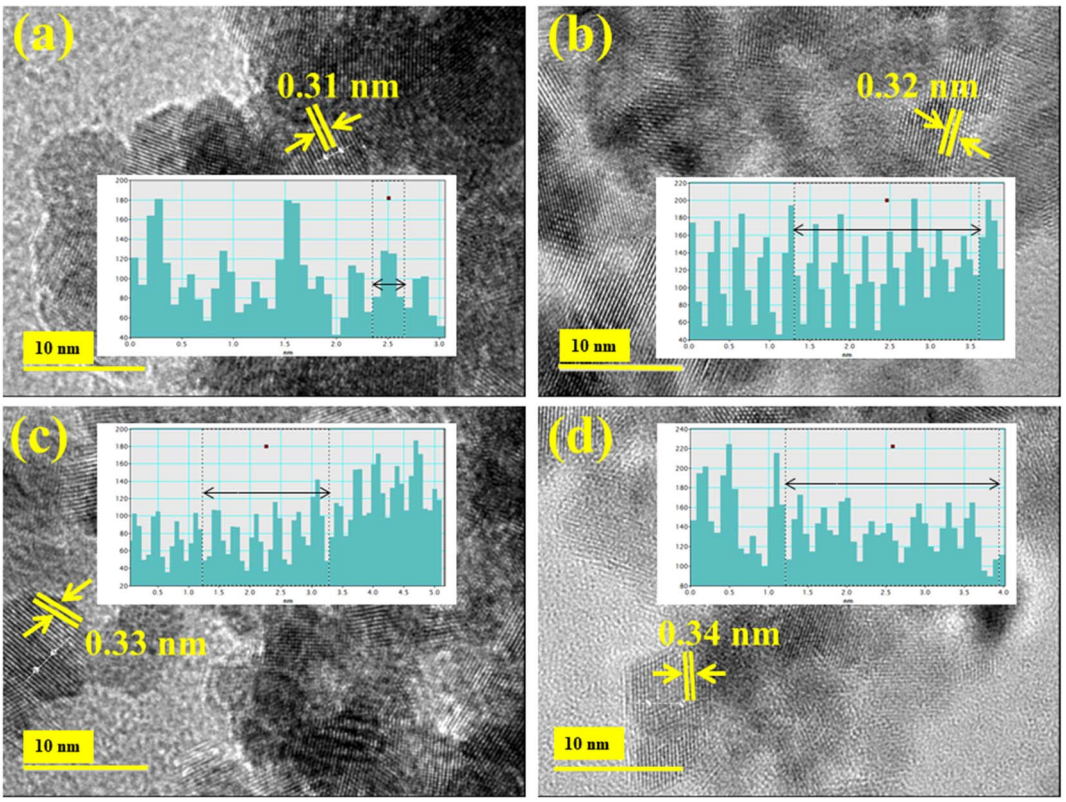

Fig. 5 (a) HRTEM analysis of (a) CeO_2 (b) PAA doped CeO_2 (c) 0.01 Ag/PAA doped CeO_2 (d) 0.03 Ag/PAA doped CeO_2.

and 82.2%, and in basic medium 52.4, 68.5, 69.3 and 70.32% for CeO_2, PAA–CeO_2, (0.01) Ag/PAA–CeO_2 and (0.03) Ag/PAA doped CeO_2, correspondingly (Fig. 6). Because of Ce variable valence state, it oxides can be changed into one another, resulting in exceptional catalytic activity. CeO_2 decreases surface area and pore volume losses, thereby enhancing the redox reaction of the catalyst.[47,48] The pH is a crucial factor in catalysis that affects the surface charges of dye molecules and catalysts. If pH is below 7 (acidic), the surface of NSs develops a positive charge, and dye becomes negative due to the ionization of the carboxyl group in RhB. This may increase the reduction of RhB dye in an acidic medium.[49] After adding Ag and PAA into CeO_2, the size of NSs reduced, which enhanced the surface area; thus, catalytic activity will increase.[50] The comparison of catalytic activity of prepared samples with traditional catalysts has been demonstrated in Table 1. The degradation efficacy of traditional materials are large and time taking, but Ag/PAA doped CeO_2 exhibit significant catalytic de-colorization of dye in 10 min.

To investigate the stability of CeO_2 and Ag/PAA doped CeO_2, an acidic degraded solution of dye was kept in the dark for 72 h to examine whether the reduction of RhB was stable or not in the existence of the prepared catalyst. The de-colorization of RhB dye was measured using UV-Vis spectrophotometer after 24 h (Fig. S3†). The obtained outcomes revealed that dye reduction efficacy was observed almost in its original form for 72 h, ensuring the stability of the catalyst.

The bactericidal activity of pure and doped CeO_2 was investigated using an agar well diffusion method in the context of MDR *E. coli* microorganisms, presented in Table 2. Inhibitory zones of pure and doped CeO_2 were observed at low and high concentrations, measured as 1.45–2.59 mm and 1.95–3.75 mm, respectively. The inhibitory zone for MDR *E. coli* was compared with a negative control DI water, which showed no inhibition (0 mm), and a positive control consisting of ciprofloxacin, which exhibited an inhibitory zone of 5.55 mm. The addition of PAA caused to increase the inhibition zones due to the presence of carboxylic and hydroxyl groups that enhanced reactive oxygen species (ROS) generation. The ROS may facilitate metal ions discharge and consequently cause bacterial cell death.[57] Furthermore, Ag doping showed a more efficient bactericidal effect, as Ag has a detrimental influence on metal oxide particle development, resulting in smaller particles and increased contact with CeO_2 NSs and bacterial cells.[50] The results demonstrated that Ag/PAA-doped CeO_2 NSs exhibited a greater bactericidal efficacy against MDR *E. coli*, a Gram-negative microorganism known for its thicker cell walls and more complex structures. The generation of oxidative stress by nanostructures depends on their shape, size, and concentration. Their size and concentration influence the antibacterial activity of particles. Smaller particles have a higher concentration of ROS, which can cause the extrusion of cytoplasmic components and lead to the death of bacteria through membrane penetration (Fig. S4†). H_2O_2 is produced when O_2 undergoes subsequent electrical reaction, creating O_2^- radicals. The hydroxyl radical ($^{\bullet}OH$) was generated when h^+ reacted with water. Therefore, the generated O_2^- and $^{\bullet}OH$ species generated

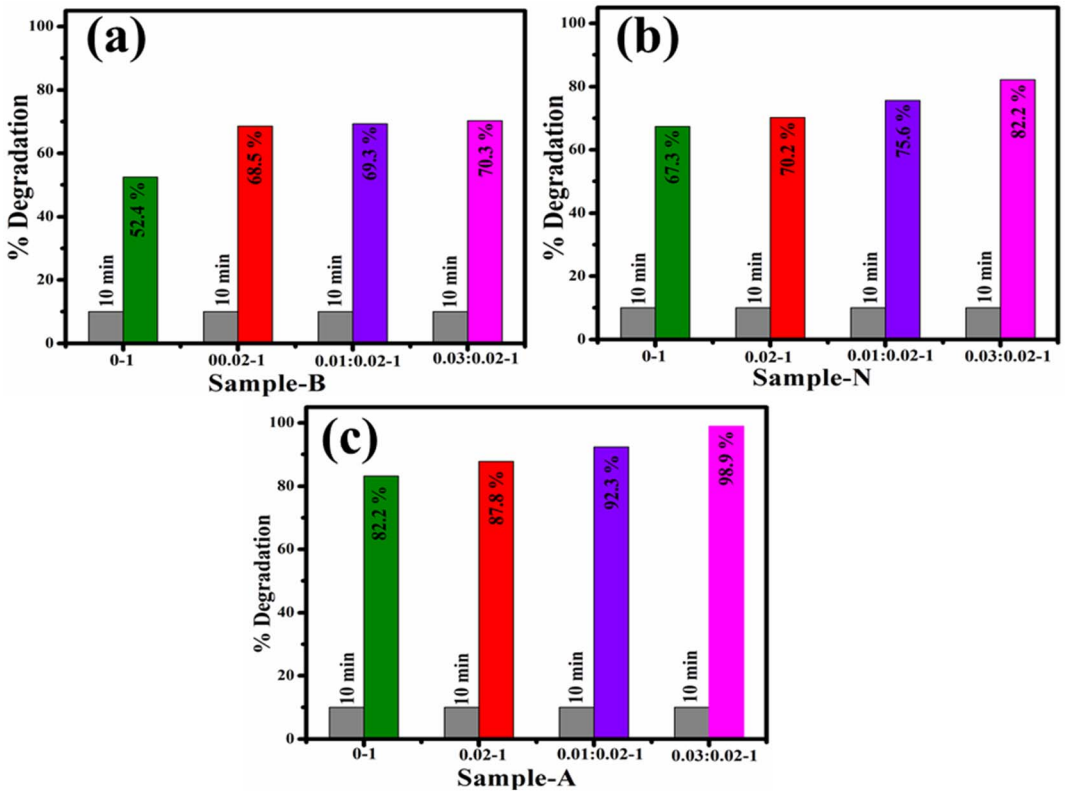

Fig. 6 Catalytic efficacy of CeO_2 and (0.01 and 0.03) Ag/PAA doped CeO_2 in various pH media (a–c).

Table 1 Comparison of prepared catalysts with traditional materials

Catalyst	Degradation efficiency (%)	Reaction time (min)	Dye (degradation condition)	Ref.
CeO_2	34.24	120	Methylene blue (visible light)	51
SnO_2	79	840	Methylene blue (visible light)	52
TiO_2	100	300	Methylene blue (visible light)	53
ZnO	85	120	Phenol (visible light)	54
WO_3	80	180	Methyl orange (visible light)	55
Au–ZnO	70	90	Methyl orange (visible light)	56
Ag/PAA doped CeO_2	98.9%	10	RhB (dark)	Present study

from the breakdown of H_2O_2 depending upon its chemical makeup and physical form perform crucial influence in the degradation of lipid or protein molecules on the bacterial cell membrane.[58,59]

Table 2 Antibacterial potential of CeO_2, and (0.01, 0.03) Ag/PAA doped CeO_2

	MDR *E. coli* inhibition zone (mm)	
Samples (Ag:PAA–CeO_2)	0.5 mg/50 μL	1.0 mg/50 μL
0–1	1.45	1.95
0.02–1	1.40	2.55
0.01:0.02–1	2.05	3.05
0.03:0.02–1	2.95	3.75
Ciprofloxacin	5.55	5.55
Deionized water (DI)	0.00	0.00

The minimum inhibitory concentrations (MICs) of CeO_2 and Ag/PAA doped NSs against MDR *E. coli* (Table 3). The results showed that the NSs shown remarkable antibacterial effectiveness against bacterial etiologies even at concentrations as low as 0.31 μg mL^{-1}. As the solution can enter the porous silica shell, the ions can completely interact with the Ag metal particles, and

Table 3 CeO_2 and Ag/PAA doped NSs MIC values against MDR *E. coli*

	MIC (μg mL^{-1})
Sample (Ag:PAA–CeO_2)	MDR *E. coli*
0–1	0.46
0.02–1	0.455
0.01:0.02–1	0.36
0.03:0.02–1	0.31

the ions may diffuse slowly, the consequence is the release of silver ions from silver cores. It seems sense to assume that these NSs would serve to stabilize Ag ions, extending the time during which they are released and ensuring that their antibacterial effects remain constant. The MIC of Ag/CNC–CeO_2 NSs against MDR *E. coli* was rather high.

Numerous research has investigated the microbicidal capability of metal-ion-containing nanoparticles.[32,60,61] The bioactivity of nanoparticles depends on their ability to interact with bacteria through electrostatic, van der Waals, or hydrophobic forces.[62,63] Docking simulations for produced nanomaterials displayed their potential linkages to residues of specified enzyme active regions. These nanocomposites exhibited modest binding energies with FabH, demonstrating their crucial interaction with essential amino acids. As indicated in Fig. S5(a–d),† docked complexes exhibited H-bonds with Leu189, Leu191 (PAA–CeO_2), and Thr81 and Gly306 (Ag/PAA–CeO_2) with binding scores of 3.60 and 5.29, respectively. Similarly, pure CeO_2 produced a stable complex (binding score of 3.23) with $FabH_{E.\ coli}$, exhibiting H-bond interactions with Cys112 and Gly306, confirming its potential function as a FabH inhibitor.

In the case of $FabI_{E.\ coli}$, synthesized NSs exhibited virtually identical binding patterns (Fig. S6a†), with pristine CeO_2 showing single H-bonds with Ala21 and Thr194 amino acids of active pocket, with a total binding score of 3.71, as shown in Fig. S6b.† PAA–CeO_2 exhibited a more robust docking complex with four hydrogen bonds inside the active region, namely Ile 20, Thr194, Leu196, and Ala196, and a binding score of 4.46 (Fig. S6c†). Similarly, the Ag/PAA–CeO_2 docked complex included three active pocket amino acid residues, namely Ile20, Ala21, and Thr165, with binding score of 4.62, depicted in Fig. S6d.†

In silico investigations are comparable to *in vitro* microbicidal efficacy for *E. coli* and recommended CeO_2 and its dopant with (PAA) and Ag/PAA as possible FabH and FabI inhibitors that should be investigated further.

4. Conclusion

In this study, CeO_2 and Ag/PAA doped CeO_2 were efficiently synthesized by co-precipitation technique to obtain significant efficacy of nanocatalyst and antibacterial. XRD spectra exhibited the cubic structure of CeO_2, and crystallinity was suppressed upon doping of Ag and PAA. The measured crystallite size reduced from 8.93 to 6.19 nm with the increasing amount of dopant into CeO_2. Electronic spectra showed the absorption increasing upon doping introduced bathochromic shift by adding Ag and PAA, which gradually decreased bandgap energy from 3.6 to 3.38 eV. TEM analysis confirmed the formation of CeO_2 nanoparticles, and the size of NPs was decreased with Ag and PAA. Among all samples, (0.03) Ag/PAA doped CeO_2 showed maximum catalytic de-colorization of 98.9% in an acidic medium. The (0.03) Ag/PAA doped CeO_2 NSs revealed substantial antibacterial efficacy and inhibition zone (3.75 mm) against *E. coli*. *In silico* estimates correlated with antibacterial activities towards *E. coli* and synthesized NSs as potential FabH and FabI inhibitors. In conclusion, Ag/PAA doped CeO_2 can be considered a good catalytic and antibacterial agent.

Data availability

Data will be available on demand.

Conflicts of interest

The manuscript is free from conflicts of interest.

Acknowledgements

The authors are thankful to higher education commission (HEC), Pakistan through NRPU-20-17615 (M. Ikram). The authors extend their appreciation to the Deanship of Scientific Research at King Khalid University, Saudi Arabia for funding this work through Small Groups Project under Grant Number (RGP.1/248/44).

References

1 F. A. Pavan, S. L. P. Dias, E. C. Lima and E. V. Benvenutti, Removal of Congo red from aqueous solution by anilinepropylsilica xerogel, *Dyes Pigm.*, 2008, **76**, 64–69, DOI: 10.1016/j.dyepig.2006.08.027.

2 G. M. Walker, L. Hansen, J. A. Hanna and S. J. Allen, Kinetics of a reactive dye adsorption onto dolomitic sorbents, *Water Res.*, 2003, **37**, 2081–2089, DOI: 10.1016/S0043-1354(02)00540-7.

3 J. b. Zhong, J. z. Li, F. m. Feng, Y. Lu, J. Zeng, W. Hu and Z. Tang, Improved photocatalytic performance of SiO 2-TiO 2 prepared with the assistance of SDBS, *J. Mol. Catal. A: Chem.*, 2012, **357**, 101–105, DOI: 10.1016/j.molcata.2012.01.026.

4 A. Ivanets, M. Roshchina, V. Srivastava, V. Prozorovich, T. Dontsova, S. Nahirniak, V. Pankov, A. Hosseini-Bandegharaei, H. N. Tran and M. Sillanpää, Effect of metal ions adsorption on the efficiency of methylene blue degradation onto MgFe 2 O 4 as Fenton-like catalysts, *Colloids Surf., A*, 2019, **571**, 17–26, DOI: 10.1016/j.colsurfa.2019.03.071.

5 M. A. Iqbal, S. I. Ali, F. Amin, A. Tariq, M. Z. Iqbal and S. Rizwan, La-and Mn-Codoped Bismuth Ferrite/Ti 3 C 2 MXene Composites for Efficient Photocatalytic Degradation of Congo Red Dye, *ACS Omega*, 2019, **4**, 8661–8668, DOI: 10.1021/acsomega.9b00493.

6 N. Al-Bastaki, Removal of methyl orange dye and Na2so4 salt from synthetic waste water using reverse osmosis, *Chem. Eng. Process.*, 2004, **43**, 1561–1567, DOI: 10.1016/j.cep.2004.03.001.

7 J. W. Lee, S. P. Choi, R. Thiruvenkatachari, W. G. Shim and H. Moon, Evaluation of the performance of adsorption and coagulation processes for the maximum removal of reactive dyes, *Dyes Pigm.*, 2006, **69**, 196–203, DOI: 10.1016/j.dyepig.2005.03.008.

8 S. S. Moghaddam, M. R. A. Moghaddam and M. Arami, Coagulation/flocculation process for dye removal using sludge from water treatment plant: optimization through response surface methodology, *J. Hazard. Mater.*, 2010, **175**, 651–657, DOI: **10.1016/j.jhazmat.2009.10.058**.

9 A. Stolz, Basic and applied aspects in the microbial degradation of azo dyes, *Appl. Microbiol. Biotechnol.*, 2001, **56**, 69–80, DOI: **10.1007/s002530100686**.

10 S. Irfan, S. Rizwan, Y. Shen, L. Li, Asfandiyar, S. Butt and C. W. Nan, The Gadolinium (Gd3+) and Tin (Sn4+) Co-doped BiFeO3 Nanoparticles as New Solar Light Active Photocatalyst, *Sci. Rep.*, 2017, **7**, 42493, DOI: **10.1038/srep42493**.

11 A. Depeursinge, D. Racoceanu, J. Iavindrasana, G. Cohen, A. Platon, P.-A. Poletti and H. Muller, Fusing Visual and Clinical Information for Lung Tissue Classification in HRCT Data, *Artif. Intell. Med.*, 2010, ARTMED1118, DOI: **10.1016/j.artmed.2010.04.006**.

12 N. Fegan, K. S. Gobius and G. A. Dykes, Pathogenic Escherichia coli, in *Encycl. Meat Sci.*, 2014, pp. 357–361, DOI: **10.1016/B978-0-12-384731-7.00035-0**.

13 M. Serhan, M. Sprowls, D. Jackemeyer, M. Long, I. D. Perez, W. Maret, N. Tao and E. Forzani, Total iron measurement in human serum with a smartphone, in *AIChE Annu. Meet. Conf. Proc.*, 2019, DOI: **10.1039/x0xx00000x**.

14 K. Kaviyarasu, P. P. Murmu, J. Kennedy, F. T. Thema, D. Letsholathebe, L. Kotsedi and M. Maaza, Structural, optical and magnetic investigation of Gd implanted CeO2 nanocrystals, *Nucl. Instrum. Methods Phys. Res., Sect. B*, 2017, **409**, 147–152, DOI: **10.1016/j.nimb.2017.02.055**.

15 K. X. Yao, X. M. Yin, T. H. Wang and H. C. Zeng, Synthesis, self-assembly, disassembly, and reassembly of two types of Cu2O nanocrystals unifaceted with {001} or {110} planes, *J. Am. Chem. Soc.*, 2010, **132**, 6131–6144, DOI: **10.1021/ja100151f**.

16 E. K. Goharshadi, S. Samiee and P. Nancarrow, Fabrication of cerium oxide nanoparticles: characterization and optical properties, *J. Colloid Interface Sci.*, 2011, **356**, 473–480, DOI: **10.1016/j.jcis.2011.01.063**.

17 M. Mittal, A. Gupta and O. P. Pandey, Role of oxygen vacancies in Ag/Au doped CeO2 nanoparticles for fast photocatalysis, *Sol. Energy*, 2018, **165**, 206–216, DOI: **10.1016/j.solener.2018.03.033**.

18 K. Suzuki, M. Kato, T. Sunaoshi, H. Uno, U. Carvajal-Nunez, A. T. Nelson and K. J. McClellan, Thermal and mechanical properties of CeO2, *J. Am. Ceram. Soc.*, 2019, **102**, 1994–2008, DOI: **10.1111/jace.16055**.

19 T. Miki, T. Ogawa, M. Haneda, N. Kakuta, A. Ueno, S. Tateishi, S. Matsuura and M. Sato, Enhanced oxygen storage capacity of cerium oxides in CeO2/La2O3/Al2O3 containing precious metals, *J. Phys. Chem.*, 1990, **94**, 6464–6467, DOI: **10.1021/j100379a056**.

20 Z. L. Wang and X. Feng, Polyhedral shapes of CeO2 nanoparticles, *J. Phys. Chem. B*, 2003, **107**, 13563–13566, DOI: **10.1021/jp036815m**.

21 H. X. Mai, L. D. Sun, Y. W. Zhang, R. Si, W. Feng, H. P. Zhang, H. C. Liu and C. H. Yan, Shape-selective synthesis and oxygen storage behavior of ceria nanopolyhedra, nanorods, and nanocubes, *J. Phys. Chem. B*, 2005, **109**, 24380–24385, DOI: **10.1021/jp055584b**.

22 T. Yu, J. Joo, Y. I. Park and T. Hyeon, Large-scale nonhydrolytic sol-gel synthesis of uniform-sized ceria nanocrystals with spherical, wire, and tadpole shapes, *Angew. Chem., Int. Ed.*, 2005, **44**, 7411–7414, DOI: **10.1002/anie.200500992**.

23 S. Tsunekawa, T. Fukuda and A. Kasuya, Blue shift in ultraviolet absorption spectra of monodisperse CeO 2-x nanoparticles, *J. Appl. Phys.*, 2000, **87**, 1318–1321, DOI: **10.1063/1.372016**.

24 M. C. Pearce and V. Thangadurai, Electrical transport properties of aliovalent cation-doped CeO2, Asia-Pacific, *J. Chem. Eng.*, 2009, **4**, 33–44, DOI: **10.1002/apj.185**.

25 T. Vinodkumar, B. G. Rao and B. M. Reddy, Influence of isovalent and aliovalent dopants on the reactivity of cerium oxide for catalytic applications, *Catal. Today*, 2015, **253**, 57–64, DOI: **10.1016/j.cattod.2015.01.044**.

26 S. R. Kanel and H. Choi, Transport characteristics of surface-modified nanoscale zero-valent iron in porous media, *Water Sci. Technol.*, 2007, **55**, 157–162, DOI: **10.2166/wst.2007.002**.

27 J. Yu, M. Lei, B. Cheng and X. Zhao, Effects of PAA additive and temperature on morphology of calcium carbonate particles, *J. Solid State Chem.*, 2004, **177**, 681–689, DOI: **10.1016/j.jssc.2003.08.017**.

28 Z. Sun, X. Wu, D. Guan, X. Chen, J. Dai, Y. Gu, S. She, W. Zhou and Z. Shao, One Pot-Synthesized Ag/Ag-Doped CeO2 Nanocomposite with Rich and Stable 3D Interfaces and Ce3+ for Efficient Carbon Dioxide Electroreduction, *ACS Appl. Mater. Interfaces*, 2021, **13**, 59993–60001, DOI: **10.1021/acsami.1c19529**.

29 D. C. McKinney, C. J. Eyermann, R. F. Gu, J. Hu, S. L. Kazmirski, S. D. Lahiri, A. R. McKenzie, A. B. Shapiro and G. Breault, Antibacterial FabH Inhibitors with Mode of Action Validated in Haemophilus influenzae by In vitro Resistance Mutation Mapping, *ACS Infect. Dis.*, 2016, **2**, 456–464, DOI: **10.1021/acsinfecdis.6b00053**.

30 M. A. Seefeld, W. H. Miller, K. A. Newlander, W. J. Burgess, W. E. DeWolf, P. A. Elkins, M. S. Head, D. R. Jakas, C. A. Janson, P. M. Keller, P. J. Manley, T. D. Moore, D. J. Payne, S. Pearson, B. J. Polizzi, X. Qiu, S. F. Rittenhouse, I. N. Uzinskas, N. G. Wallis and W. F. Huffman, Indole naphthyridinones as inhibitors of bacterial enoyl-ACP reductases FabI and FabK, *J. Med. Chem.*, 2003, **46**, 1627–1635, DOI: **10.1021/jm0204035**.

31 Z. Mehmood, M. Ikram, M. Imran, A. Shahzadi, A. Haider, A. Ul-Hamid, W. Nabgan, J. Haider and S. Hayat, Z. officinale-doped silver/calcium oxide nanocomposites: catalytic activity and antimicrobial potential with molecular docking analysis, *Process Biochem.*, 2022, **121**, 635–646, DOI: **10.1016/j.procbio.2022.07.035**.

32 S. Altaf, A. Haider, S. Naz, A. Ul-Hamid, J. Haider, M. Imran, A. Shahzadi, M. Naz, H. Ajaz and M. Ikram, Comparative Study of Selenides and Tellurides of Transition Metals (Nb and Ta) with Respect to its Catalytic, Antimicrobial, and

Molecular Docking Performance, *Nanoscale Res. Lett.*, 2020, **15**, 1–16, DOI: 10.1186/s11671-020-03375-0.

33 C.-W. Liew, H. M. Ng, A. Numan and S. Ramesh, Poly(Acrylic acid)–Based Hybrid Inorganic–Organic Electrolytes Membrane for Electrical Double Layer Capacitors Application, *Polymers*, 2016, **8**, 179, DOI: 10.3390/polym8050179.

34 P. Maleki, F. Nemati, A. Gholoobi, A. Hashemzadeh, Z. Sabouri and M. Darroudi, Green facile synthesis of silver-doped cerium oxide nanoparticles and investigation of their cytotoxicity and antibacterial activity, *Inorg. Chem. Commun.*, 2021, **131**, 108762, DOI: 10.1016/j.inoche.2021.108762.

35 G. Jayakumar, A. A. Irudayaraj and A. D. Raj, Investigation on the synthesis and photocatalytic activity of activated carbon–cerium oxide (AC–CeO2) nanocomposite, *Appl. Phys. A: Mater. Sci. Process.*, 2019, **125**, 742, DOI: 10.1007/s00339-019-3044-4.

36 E. Kumar, P. Selvarajan and K. Balasubramanian, Preparation and studies of cerium dioxide(CeO 2) nanoparticles by microwave-assisted solution method, *Recent Res. Sci. Technol.*, 2010, **2**, 37–41.

37 D. Girija, H. S. B. Naik, C. N. Sudhamani and B. V. Kumar, Cerium oxide nanoparticles - a green, reusable, and highly efficient heterogeneous catalyst for the synthesis of Polyhydroquinolines under solvent-free conditions, *Appl. Sci. Res.*, 2011, **3**, 373–382.

38 Á. G. Aponte, M. A. L. RamÍrez, Y. C. Mora, J. F. Santa MarÍn and R. B. Sierra, Cerium oxide nanoparticles for color removal of indigo carmine and methylene blue solutions, *AIMS Mater. Sci.*, 2020, **7**, 468–485, DOI: 10.3934/matersci.2020.4.468.

39 M. Chelliah, J. B. B. Rayappan and U. M. Krishnan, Synthesis and characterization of cerium oxide nanoparticles by hydroxide mediated approach, *J. Appl. Sci.*, 2012, **12**, 1734–1737, DOI: 10.3923/jas.2012.1734.1737.

40 A. Miri, M. Darroudi and M. Sarani, Biosynthesis of cerium oxide nanoparticles and its cytotoxicity survey against colon cancer cell line, *Appl. Organomet. Chem.*, 2020, **1**, e5308, DOI: 10.1002/aoc.5308.

41 Z. C. Orel and B. Orel, Optical Properties of Pure CeO2 and Mixed CeO2/SnO2 Thin Film Coatings, *Phys. Status Solidi*, 1994, **186**, K33–K36, DOI: 10.1002/pssb.2221860135.

42 S. Chahal, S. Singh, A. Kumar and P. Kumar, Oxygen-deficient lanthanum doped cerium oxide nanoparticles for potential applications in spintronics and photocatalysis, *Vacuum*, 2020, **177**, DOI: 10.1016/j.vacuum.2020.109395.

43 B. Jain, A. K. Singh, A. Hashmi, M. A. B. H. Susan and J. P. Lellouche, Surfactant-assisted cerium oxide and its catalytic activity towards Fenton process for non-degradable dye, *Adv. Compos. Hybrid Mater.*, 2020, **3**, 430–441, DOI: 10.1007/s42114-020-00159-z.

44 R. C. Deus, J. A. Cortés, M. A. Ramirez, M. A. Ponce, J. Andres, L. S. R. Rocha, E. Longo and A. Z. Simões, Photoluminescence properties of cerium oxide nanoparticles as a function of lanthanum content, *Mater. Res. Bull.*, 2015, **70**, 416–423, DOI: 10.1016/j.materresbull.2015.05.006.

45 S. Moeen, M. Ikram, A. Haider, J. Haider, A. Ul-Hamid, W. Nabgan, T. Shujah, M. Naz and I. Shahzadi, Comparative Study of Sonophotocatalytic, Photocatalytic, and Catalytic Activities of Magnesium and Chitosan-Doped Tin Oxide Quantum Dots, *ACS Omega*, 2022, **7**, 46428–46439, DOI: 10.1021/acsomega.2c05133.

46 F. Maillard, S. Schreier, M. Hanzlik, E. R. Savinova, S. Weinkauf and U. Stimming, Influence of particle agglomeration on the catalytic activity of carbon-supported Pt nanoparticles in CO monolayer oxidation, *Phys. Chem. Chem. Phys.*, 2005, 375–383, DOI: 10.1039/b411377b.

47 Y. Chen, C. Chen, Y. Liu and L. Yu, Probing the effect of nitrate anion in CAN: an additional opportunity to reduce the catalyst loading for aerobic oxidations, *Chin. Chem. Lett.*, 2023, 108489, DOI: 10.1016/j.cclet.2023.108489.

48 M. Cai, X. Bian, F. Xie, W. Wu and P. Cen, Preparation and performance of cerium-based catalysts for selective catalytic reduction of nitrogen oxides: a critical review, *Catalysts*, 2021, **11**, 1–23, DOI: 10.3390/catal11030361.

49 T. S. Natarajan, M. Thomas, K. Natarajan, H. C. Bajaj and R. J. Tayade, Study on UV-LED/TiO2 process for degradation of Rhodamine B dye, *Chem. Eng. J.*, 2011, **169**, 126–134, DOI: 10.1016/j.cej.2011.02.066.

50 F. Jamal, M. Ikram, A. Haider, A. Ul-Hamid, M. Ijaz, W. Nabgan, J. Haider and I. Shahzadi, Facile synthesis of silver and polyacrylic acid doped magnesium oxide nanostructure for photocatalytic dye degradation and bactericidal behavior, *Appl. Nanosci.*, 2022, **12**, 2409–2419, DOI: 10.1007/S13204-022-02504-8.

51 A. Shahzadi, S. Moeen, A. D. Khan, A. Haider, J. Haider, A. Ul-Hamid, W. Nabgan, I. Shahzadi, M. Ikram and A. Al-Shanini, La-Doped CeO2 Quantum Dots: Novel Dye Degrader, Antibacterial Activity, and In Silico Molecular Docking Analysis, *ACS Omega*, 2023, **8**, 8605–8616, DOI: 10.1021/acsomega.2c07753.

52 S. P. Kim, M. Y. Choi and H. C. Choi, Photocatalytic activity of SnO2 nanoparticles in methylene blue degradation, *Mater. Res. Bull.*, 2016, **74**, 85–89, DOI: 10.1016/j.materresbull.2015.10.024.

53 P. Ren, M. Song, J. Lee, J. Zheng, Z. Lu, M. Engelhard, X. Yang, X. Li, D. Kisailus and D. Li, Edge Dislocations Induce Improved Photocatalytic Efficiency of Colored TiO2, *Adv. Mater. Interfaces*, 2019, **6**, 1901121, DOI: 10.1002/admi.201901121.

54 M. C. Uribe-López, M. C. Hidalgo-López, R. López-González, D. M. Frías-Márquez, G. Núñez-Nogueira, D. Hernández-Castillo and M. A. Alvarez-Lemus, Photocatalytic activity of ZnO nanoparticles and the role of the synthesis method on their physical and chemical properties, *J. Photochem. Photobiol., A*, 2021, **404**, 112866, DOI: 10.1016/j.jphotochem.2020.112866.

55 M. Qamar, Z. H. Yamani, M. A. Gondal and K. Alhooshani, Synthesis and comparative photocatalytic activity of Pt/WO3 and Au/WO3 nanocomposites under sunlight-type

excitation, *Solid State Sci.*, 2011, **13**, 1748–1754, DOI: 10.1016/j.solidstatesciences.2011.07.002.

56 K. X. Yao, X. Liu, L. Zhao, H. C. Zeng and Y. Han, Site-specific growth of Au particles on ZnO nanopyramids under ultraviolet illumination, *Nanoscale*, 2011, **3**, 4195–4200, DOI: 10.1039/c1nr10685f.

57 M. Ikram, A. Haider, M. Imran, J. Haider, S. Naz, A. Ul-Hamid, A. Shahzadi, S. Moeen, G. Nazir, W. Nabgan, A. Bashir and S. Ali, Cellulose grafted poly acrylic acid doped manganese oxide nanorods as novel platform for catalytic, antibacterial activity and molecular docking analysis, *Surf. Interfaces*, 2023, **37**, 102710, DOI: 10.1016/j.surfin.2023.102710.

58 P. I. Rajan, J. J. Vijaya, S. K. Jesudoss, K. Kaviyarasu, L. J. Kennedy, R. Jothiramalingam, H. A. Al-Lohedan and M. A. Vaali-Mohammed, Green-fuel-mediated synthesis of self-assembled NiO nano-sticks for dual applications-photocatalytic activity on Rose Bengal dye and antimicrobial action on bacterial strains, *Mater. Res. Express*, 2017, **4**, 085030, DOI: 10.1088/2053-1591/aa7e3c.

59 Z. Wang, M. Liu, F. Xiao, G. Postole, H. Zhao and G. Zhao, Recent advances and trends of heterogeneous electro-Fenton process for wastewater treatment-review, *Chin. Chem. Lett.*, 2022, **33**, 653–662, DOI: 10.1016/j.cclet.2021.07.044.

60 M. V. Arularasu, M. Harb and R. Sundaram, Synthesis and characterization of cellulose/TiO2 nanocomposite: evaluation of in vitro antibacterial and in silico molecular docking studies, *Carbohydr. Polym.*, 2020, **249**, 116868.

61 M. Ikram, J. Hassan, A. Raza, A. Haider, S. Naz, A. Ul-Hamid, J. Haider, I. Shahzadi, U. Qamar and S. Ali, Photocatalytic and bactericidal properties and molecular docking analysis of TiO2nanoparticles conjugated with Zr for environmental remediation, *RSC Adv.*, 2020, **10**, 30007–30024, DOI: 10.1039/d0ra05862a.

62 I. Shahzadi, M. Islam, H. Saeed, A. Haider, A. Shahzadi, J. Haider, N. Ahmed, A. Ul-Hamid, W. Nabgan, M. Ikram and H. A. Rathore, Formation of biocompatible MgO/cellulose grafted hydrogel for efficient bactericidal and controlled release of doxorubicin, *Int. J. Biol. Macromol.*, 2022, **220**, 1277–1286, DOI: 10.1016/j.ijbiomac.2022.08.142.

63 T. C. Dakal, A. Kumar, R. S. Majumdar and V. Yadav, Mechanistic basis of antimicrobial actions of silver nanoparticles, *Front. Microbiol.*, 2016, **7**, 1831, DOI: 10.3389/fmicb.2016.01831.